12,18

Graphene/nanotube quasi-1D structures in strong electric fields

© O.E. Glukhova, M.M. Slepchenkov

Saratov State University,
Saratov, Russia

E-mail: glukhovaoe@info.sgu.ru

Received December 26, 2021
Revised January 21, 2022
Accepted January 21, 2022

In silico studies of the behavior of graphene/nanotube quasi-one-dimensional (1D) structures with covalent bonded graphene and nanotube in strong electric fields with a strength of 10^7-10^8 V/cm have been carried out. The atomic structure, band structure, electron transmission function, electrical conductivity, and regularity of the electronic structure changes in strong fields have been studied. It is found that the electron transmission function of quasi-1D structures has an intensity peak at the Fermi level in contrast to nanotubes and graphene. As a result of quantum molecular dynamics modeling, the regularities of deformation of the atomic framework and its destruction under the action of ponderomotive force have been established. We have found a critical value of the strength at which the electric field detaches the graphene from the tube. It is $\sim 2 \cdot 10^8$ V/cm. A further increase leads to the detachment of graphene from the tube with its simultaneous destruction.

Keywords: graphene/nanotube structures, electrical conductivity, ponderomotive force, strong electric fields.

DOI: 10.21883/PSS.2022.05.53519.264

1. Introduction

Carbon nanotubes (CNT) and graphene have attracted the attention of researchers all over the world over the past decades because of their unique physical properties, including large specific surface area, high electrical and thermal conductivity, carrier mobility, transparency, micromechanical strength and flexibility [1–3]. Combination of CNT and graphene in hybrid structures opens the ways to production of new materials with promising properties due to the synergistic effect of combining multi-sized structures [4–10]. The existing topological configurations of graphene-nanotube hybrid material include two major groups: hybrid structures with horizontally-aligned CNT [11–16] and vertically-aligned CNT [17–21]. Hybrid structures with vertically-aligned CNT sometimes referred to as „pillared graphene“ are used in the manufacture of battery electrodes [22], phonon device components [23] and nanomechanical sensors [24] as well as a gas separation membrane [25] and thermal interface materials [26]. Based on graphene/horizontally-aligned CNT hybrid structures, high-sensitivity photodetectors [27], humidity sensors [28], gas sensors [29], lithium-ion batteries [30] and supercapacitors [31] are developed.

The research focused on production of compounds from covalent-bonded nanotubes and graphene is of great interest [17–21,32–34]. Such compounds have improved electrical and physical properties as compared with that of atomically thin graphene [32]. To identify the influence patterns of the atomic structure features on the covalent-bonded graphene-CNT composite properties and to forecast their potential applications, computer-based simulation methods are widely used [35–48]. In particular, some papers address CNT-graphene heterostructures with zigzag-type (12,0) or (8,0) horizontally-aligned single-walled carbon nanotubes (SWCNT) covalent bonded with one or more graphene nanoribbons with a width equal to the SWCNT length [38–40]. In this type of structures, sp^3-hybridized bond is formed at the tube-graphene interface thanks to which graphene-SWCNT composite has a much higher Young's modulus as compared with a nanotube and graphene separately, demonstrates Van Hove peaks in electron density distribution, and opening of a band gap of several hundred of eV when a nanoribbon and nanotube comes in contact with semiconductor type conductivity. There are quite a lot theoretical papers devoted to the simulation of CNT-graphene seamless heterostructures with vertically-aligned nanotubes and to the investigation of their electronic and thermal conductivity properties [42–48]. The paper [43] offers various topological options for tube-based CNT-graphene heterostructures (6,6), including configurations with open- or closed-ended nanotubes. Using the tight-binding method, the authors forecast that despite the metallic nature of conductivity of CNT (6,6) and graphene sheet, CNT(6,6)-graphene heterostructures are characterized by the presence of 0.27 eV (with open-ended CNT) and 0.51 meV (closed-ended CNT) band gap. A similar effect of the presence of a 0.2 eV band gap was found for a 3D-grid formed by CNT (5,5) integrated into a graphene sheet on both sides [44]. In [45], *ab initio* methods are used to investigate the transport properties of pillared graphene based on armchair (4,4) and zigzag (8,0) nanotubes. It has been found that for column graphene based on metallic CNTs (4,4) conductivity is essentially independent of the tube length, but changes drastically depending on the graphene-CNT contact structure, while

for pillared graphene based on semiconductor CNTs (8,0), conductivity is mainly defined by the tube length and is independent on the graphene-CNT contact structure. As illustrated by atomistic models of CNT (6,6)-based pillared graphene in [46–48], seamless 3D-graphene-CNT structures show outstanding thermal conductivity properties with heat flux defined in such structures by the minimum distance between the tubes and tube lengh [47].

In recent years, one of the promising areas of graphene-CNT research included production of composite materials with improved emission characteristics for further use as nano-emitters [49–54]. One of the latest achievements in this area was the experimental electrophoretic deposition of SWCNT/graphene hybrid films demonstrating the maximum emission current of 80 mA with the corresponding current density of 160 mA/cm^2 at an electric field strength of 9.6 V/μm [54]. At the same time, this and other papers do not address the behavior of graphene/CNT hybrid structures in strong electric fields with a strength of 10^9-10^{10} V/m that is typical of the emissive centers of field radiating cathodes. Understanding of this issue is essential for successful application of graphene-nanotube films as an electron emitter in vacuum electron devices.

This paper is devoted to *in silico* study of the influence of strong electric fields with a strength of 10^7-10^8 V/cm and higher on the atomic and electronic configuration of quasi-1D-structures based on chiral nanotube (6,5) and graphene covalent bonded with the tube. The object of simulation has been chosen because such covalent-bonded graphene-CNT structures can be synthesized in a real experiment, in particular, using the laser nanowelding technique [55].

2. Mathematical simulation: approaches and methods

Atomistic models of graphene/nanotube quasi-1D-structures were built first. A self-consistent charge density functional tight-binding method (SCC DFTB, non-spin-polarized) implement in DFTB+ software suite [56] was used for simulation. An equilibrium configuration of thin film super cells was achieved by minimizing the total energy during variation of all super cell atom coordinates and super cell translation vector length. For this, Monkhorst–Pack approach [57] was used to draw the first Brillouin zone and the investigations were carried out using a $1 \times 4 \times 1$ grid (periodic structure towards axis Y). Electron population was studied at 300 K and defined by Fermi–Dirac function

$$f(\varepsilon) = \left[1 + \exp(\varepsilon/k_B T)\right]^{-1}. \quad (1)$$

To consider a potential Van der Waals interaction (attraction—repulsion) between separate structural elements of quasi-1D-structures within the SCC DFTB method, a universal force field (UFF) potential was used [58]. To identify the electronic structure patterns, density of electronic states (DOS) and Fermi energy were calculated. To study electric conductivity of quasi-1D-structures, nonequilibrium Green's–Keldysh's function approach and Landauer–Butiker formalism were used [59] to determine the conductivity G based on the electron transmission function $T(E)$:

$$G = \frac{2e^2}{h} \int_{-\infty}^{\infty} T(E) F_T(E - E_F) dE, \quad (2)$$

where e is the electron charge, h is the Planck constant. e^2/h is the conductance quantum. The conductance quantum value is doubled to consider the electron spin. The thermal broadening function $F_T(E)$ is calculated using the equation:

$$F_T(E) = \frac{1}{4k_B T} \operatorname{sech}\left(\frac{E}{2k_B T}\right), \quad (3)$$

where k_B is the Boltzmann's constant, T is the temperature. As known, the electron transmission function $T(E)$ characterizes the quantum-mechanical transparency of the conduction channel (a structure segment enclosed between two contacts) depending on the energy of an electron moving in it. The structure super cell serves as a channel and semi-infinite structures, obtained by means of the structural super cell translation in two opposite directions, serve as electrodes. The formalism describes the electron transport patterns when only elastic collisions with the crystal lattice atoms are considered during the electron movement via the channel. The energy was also calculated using the SCC DFTB method. The structural behavior in the electric field was identified using the Born–Oppenheimer quantum molecular dynamics based on the SCC DFTB method with the augmented Lagrangian method [60]. This is a comparatively new method and is an alternative approach to the quantum molecular dynamic simulation. It is based on the augmented Lagrangian formulation of the Born–Oppenheimer molecular dynamics [61] and makes it possible to avoid the disadvantages of the previous molecular dynamics modifications by combining some best features of the Car–Parrinello and Born–Oppenheimer approaches. A time interval of 0.5 fs was used for the calculations.

3. Atomistic models

To build the atomistic models of graphene/nanotube quasi-1D-structures, chiral nanotube (6,5) and graphene fragments were chosen. The tube (6,5) was selected because it is one of the commonly synthesized single-walled tubes with a subnanometer diameter of 0.75 nm. The traslation vector length is $L_y = 4.064$ nm. Two models were derived from this tube. One of the models (Q1D-1) containing 722 atoms is shown in Fig. 1, *a*. A graphene flake contains 358 atoms, a tube contains 364 atoms. The initial translation vector length of the quasi-1D-structure Q1D-1

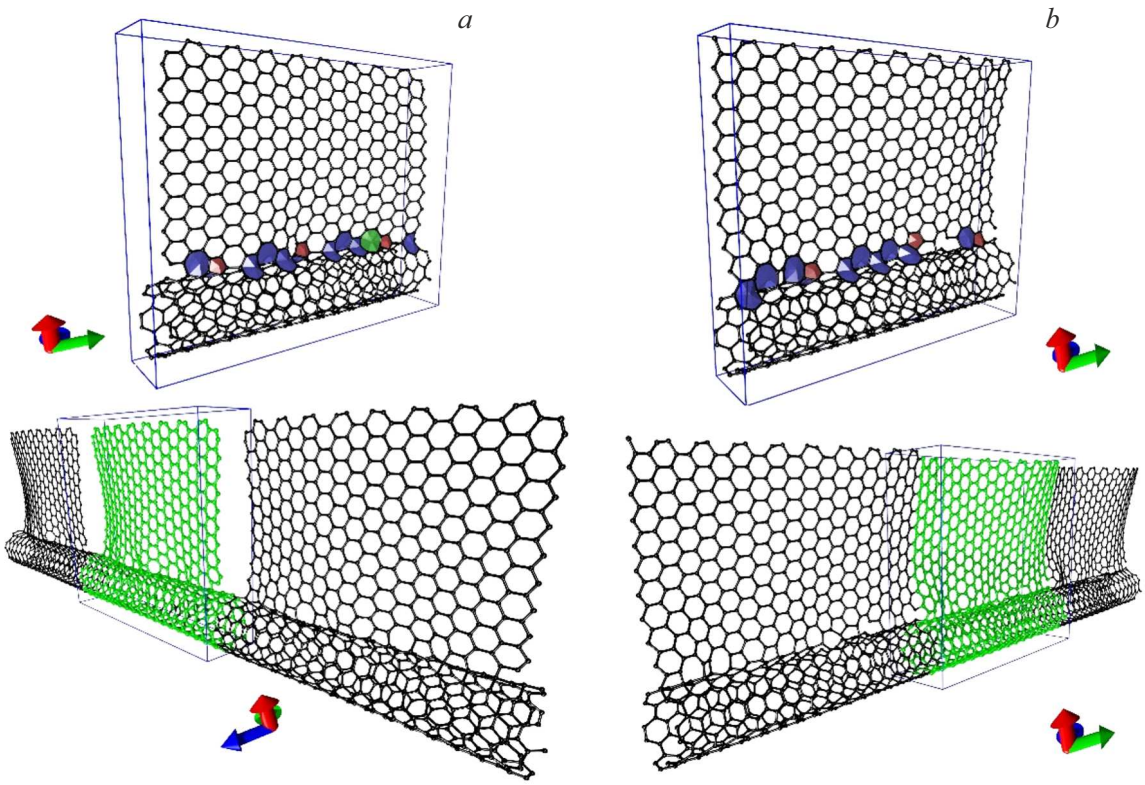

Figure 1. Atimistic models of a quasi-1D-structure with graphene flakes: (*a*) Q1D-1; (*b*) Q1D-2.

corresponded to the calculated individual tube period (6,5). The smallest distance between the graphene and tube atoms was ~ 1.65 Å. As a result of optimization, the tube and graphene formed covalent bonds. The number of atoms in the super cell remained unchanged. The bond lengths and the super cell translation vector length changed. There are non-hexagonal elements at the interface, as shown in Fig. 1, *a* (on the top): pentagons, heptagons and octagons. The pentagons are red, heptagons are blue and octagons are green. It can be immediately seen that the non-hexagonal elements are distributed unevenly along the atomic structure of the nanotube which is due to the chiral structure of the tube that prevents the occurrence of similar covalent bonds throughout the graphene length. So, a group of septagons/octagons/pentagons was detected near one tube end at the graphene-nanotube interface, but there no octagons at all and the number of septagons/pentagons is significantly lower near the other tube end. The pentagons are red, heptagons are blue and octagon is green. The same Figure 1, *a* (on the bottom) shows a fragment of an infinite quasi-1D-structure with a periodic box (the periodic box is blue and the super cell atoms are green). This Figure shows the quasi-1D-structure view such that to allow a better topology presentation. Actually, it can be seen that the graphene flakes are as if repulsed from each other and form a free space between them. The distance between the adjacent graphene flake atoms is ~ 5.6 Å and more. The repulsion of the graphene flakes from each other causes the increase in the structure length and the translation vector length after the optimization is 4.09 nm. Thus, the topology of the first quasi-1D-structure (Q1D-1) model is characterized in some regions by the absence of covalent bonds between the graphene ribbon and nanotube. All topological and metric characteristics are listed in Table 1.

The other model (Q1D-2) built on the same nanotube (6,5) differs in that the graphene is presented by a solid 1D-nanoribbon covalently bonded to the nanotube. The initial atomistic model of the super cell had a translation vector length equal to $L_y = 4.064$ nm, the smallest distance between the graphene and tube atoms was also ~ 1.65 Å. The number of tube atoms (6,5) remained unchanged, but the number of graphene flake atoms was increased up to 380. This means that the graphene flake length was made as much close as possible to the length of the initial individual tube to form covalent bonds not only between the graphene and tube, but also between the adjacent graphene flakes. Because of the tube chirality (6,5), no homogeneous graphene–tube bond and planar graphene nanoribbon topology along the tube can be achieved, but corrugated graphene bonded with the tube may be obtained. This was achieved. Fig. 1, *b* shows atomistic model of the quasi-1D-structure with an extended graphene sheet covalently bonded to the nanotube that was achieved as a result of the optimization. The same Figure shows non-hexagonal elements at the graphene–tube interface. This model is characterized by the appearance of pentagons

Table 1. The geometrical and energy parameters of the graphene/nanotube quasi-1D-structures super cell

Parameters	Q1D-1	Q1D-2
Number of pentagons	5	6
Number of heptagons	11	8
Number of octagons	2	0
Graphene-CNT covalent bond length, Å	1.56	1.57
Structure length along axis X, Å	33.00	33.12
Translation vector L_y, Å	40.90	40.64
Formation energy, eV/atom	−47.14	−47.18

and heptagons, but without octagons. Nonsymmetrical distribution of non-hexagonal elements at the graphene and nanotube interface is also typical. Fig. 1, *b* shows an extended quasi-1D-structure fragment with a super cell shown in green. It can be seen that the extended graphene ribbon fragment is irregularly bonded with the nanotube, i.e. there are regions without graphene−nanotube covalent bonds. As previously mentioned, this can be expected due to the chiral structure of the atomic tube core. All topological and metric characteristics of Q1D-2 model are listed in Table 1. It should be noted that the translation vector length remained unchanged after the optimization, but the graphene sheet lost one atom when the tube bonds were formed and a result a pentagon was formed in the center. Thus, the super structure contained 743 atoms instead of 744-atoms. This allowed to achieve the graphene/nanotube structure that is as close to the synthesized structures as possible in terms of topology.

Table 1 shows that the bond lengths at the graphene and interface correspond to sp^3-hybridization state because the atoms in this region form 4 valent bonds. It is also seen that the quasi-1D-structure with the extended graphene sheet predominantly bonded to the extended tube (6,5) is the most energetically favorable option. This may be explained by the fact that the graphene flakes (Fig. 1, *a*) are repulsed from each other and cause some kind of stress in the atomic structure. And despite the graphene corrugation in Q1D-2 model, the bond lengths are within the values typical of graphene and are equal to 1.40−1.42 Å. Generally, both models are energetically favorable in terms of their formation because the formation energy calculated as the difference of energies of the final structure and separate initial fragments is negative.

4. Electronic and electrophysical characteristics

For the built quasi-1D-structures, densities of electronic states and Fermi energy were calculated and electronic transportation properties were investigated by calculation of the transmission function $T(E)$, then conduction G and resistance. Fig. 2, *a* shows the curves of the density of electronic states for both quasi-1D-structure models as well as the Fermi energy values significantly different for the two models. Fig. 2, *b* shows the transmission function curves. The electronic and electrophysical parameters of the studied quasi-1D-structures are listed in Table 2. The Fermi energy for Q1D-2 model with the extended graphene ribbon sheet is close to that for the pure graphene monolayer (4.61 eV), band gap is virtually absent in the band structure. For graphene flake option Q1D-1, the Fermi energy is more compliant with that for individual nanotubes, but the band gap is also negligible. Both curves of densities of electronic states do not display any bad gap. Thus, a very interesting physical fact was found which needs to be discussed and understood: when the initial individual chiral tube (6,5) and „armchair"-type graphene ribbon have a band gap, the quasi-1D-structures become conductive.

To explain this effect, electronic characteristics of the individual extended chiral tube (6,5) and „armchair" extended graphene nanoribbon, whose fragments were used to form graphene/nanotube quasi-1D-structures, were investigated. As shown in Fig. 1, AGNR armchair-type nanoribbon served as an extended graphene ribbon and contacted with the tube. One nanoribbon was chosen for both models, but a flake, i.e. a part of the ribbon, was taken for Q1D-1 model, and an extended nanoribbon was taken for Q1D-2 model. The band gap of the individual tube (6,5) band structure is 0.9 eV, the Fermi energy is −4.57 eV. The graphene nanoribbon has a 1 eV band gap (without edge passivation) with the Fermi energy equal to −5.72 eV. The graphene structure edges were not passivated herein, therefore the graphene nanoribbon was assumed as unpassivated. As can be seen, both initial structures are of semiconductor type, and, on the other hand, both of them have only sp^2-hybridized electron clouds for all atoms. When a hybrid graphene/nanotube structure is formed, sp^3-hybridization of the atom electron clouds is observed and as a result the charge partially flows from the tube to the graphene ribbon.

First, consider the second Q1D-2 structure with the extended graphene ribbon rather than a flake-type ribbon. In this case, partial charge flow from the tube to the contacting graphene nanoribbon is observed. Such charge flow is rather conditional because there is a graphene−nanotube covalent bond, but in this case these fragments are studied separately in order to characterize the observed electronic density redistribution somehow. So, the graphene charge is $\sim -0.82e$ (e the absolute electron charge) and this value is typical of a super cell, i.e. charge flow from the tube to the graphene is observed throughout the structure. While all atoms forming covalent bond with the graphene have a lack of charge $\sim 0.13-0.14e$. As known, Mulliken has previously proposed to assess the electron density distribution over the structural atoms in the electron charge units. This approach helps to understand where local regions with excessive electron charge are present. Such approach certainly does not mean that a half of charge has flown from the tube to the graphene, but the electron charge density redistribution is implied, i.e. a density

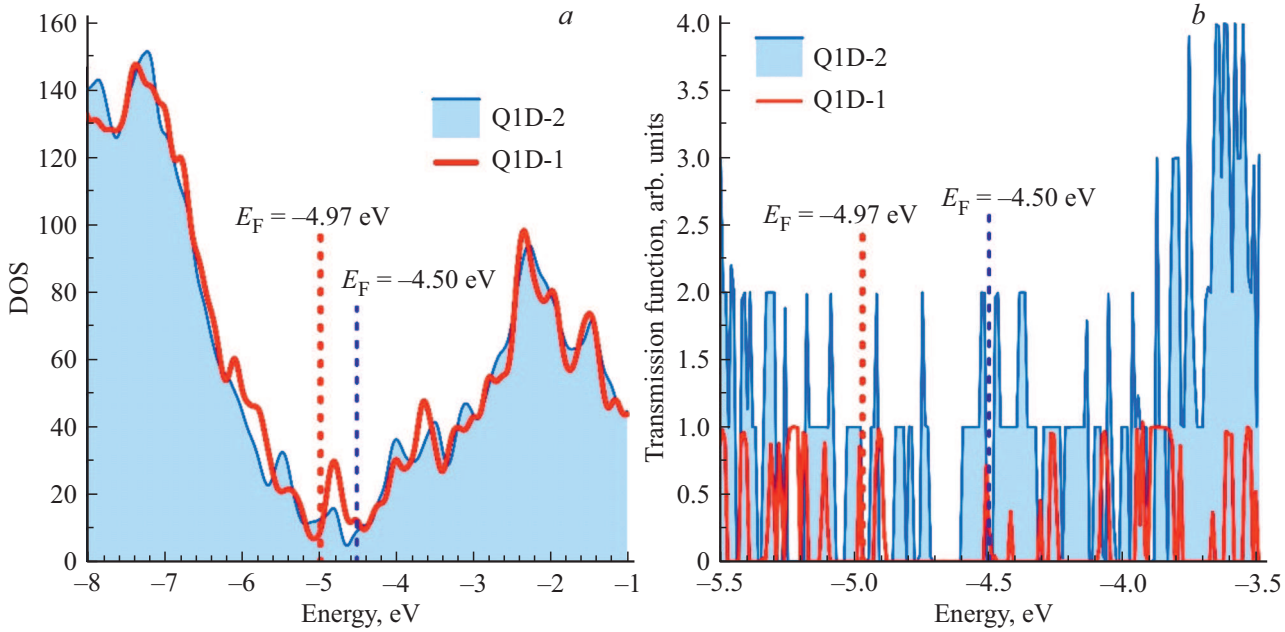

Figure 2. Curves of the density of electronic states (a) and transmission function (b) of graphene/nanotube quasi-1D-structures.

Table 2. Electronic and electrophysical characteristics of graphene/nanotube quasi-1D-structures

Parameters	Q1D-1	Q1D-2
Fermi energy, eV	−4.97	−4.50
Band gap, eV	0.08	0.04
Conductivity, μS	13.064	78.400
Resistance, kOhm	76.545	12.755

probability map calculation for the total graphene/ nanotube structure electron cloud. Coming back to the foregoing, we shall note that the graphene ribbon covalently bonded to the nanotube has an excessive electron charge which significantly changes the electronic properties of the whole quasi-1D-structure. Therefore, the density of electronic states near the Fermi level on both sides (Fig. 2, b) is non-zero and the transmission function curve shows two intensity peaks at level „2“. The transmission function is given in relative units — conductance quanta e^2/h. Thus, the resistance of the produced graphene/nanotube quasi-1D-structure is rather low (Table 2, only $\sim 12.8\,\text{k}\Omega$, which is close to that of the ideal „armchair“-type tubes $6.4\,\text{k}\Omega$. The other structure Q1D-1 is characterized by a higher resistance, the Fermi level is offset to the lower value range (Table 2). The transmission function profile is absolutely different from that for Q1D-2 structure. There is an intensity peak near the Fermi level, but its value is equal to 1, and as curve $T(E)$ shows, the transmission function intensity does not achieve „2“ throughout the energy interval. Such result for Q1D-1 structure can be expected. Thus, for example, graphene flakes can not take a high charge, but only $\sim -0.58e$ (per super cell).

Summing up the electronic structure data, it can be concluded that a new complex formed by the graphene nanoribbon/flakes and nanotube brings a brand-new electronic structure to the complex which differs from that of both the nanotube and graphene nanoribbon.

5. Behavior in strong electric fields

The behavior of quasi-1D-structures in strong electric fields which are required for field emission was further investigated. First of all, critical fields that will destroy the structure shall be identified. The quasi-1D-structure is arranged herein such that it represents a field-emission edge cathode. The force line directions are shown in Fig. 3. The external field causes the electron charge density redistribution in the structure. Obviously, the maximum excessive charge is observed at the edge graphene atoms (shown in blue), i.e. the field as if „pulls“ the electron charge from the whole structure to the edge. Behavior in the fields with a strength from $1 \cdot 10^7$ to $2 \cdot 10^8$ V/cm was studied. It was found that partial demolition begins at $1.5 \cdot 10^8$ V/cm which is shown in Fig. 3. Fig. 3, a, b shows the electron charge density distribution map and atomic grid of Q1D-1 model with a graphene flake. Partial demolitions take place as early as during the first picosecond from the external field activation time. Fig. 3, b shows that the flake is almost completely separated from the nanotube by the field and the tube itself has local breakdown of covalent bonds in the separation area (these areas are shown in blue). A similar situation is also observed for the other Q1D-2 model (Fig. 3, c, d). At the same field strength, graphene in

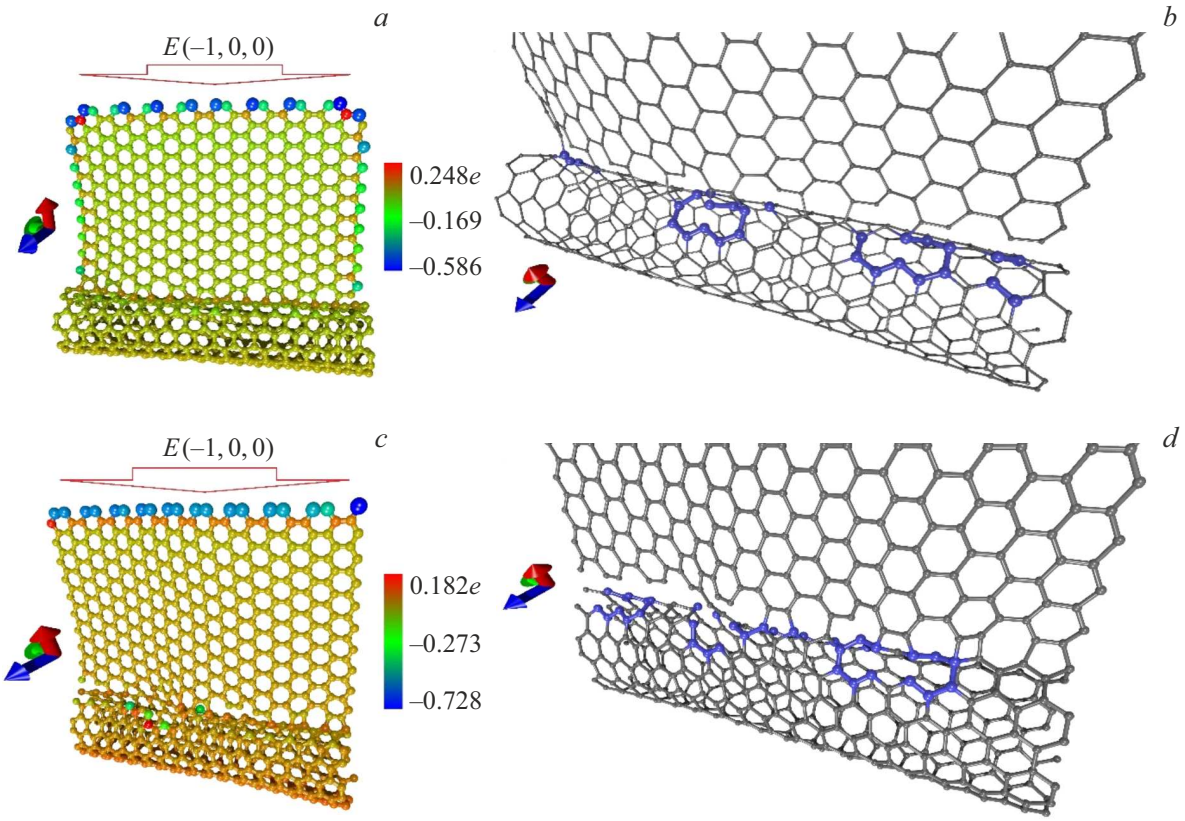

Figure 3. Quasi-1D-structures in the electric field with a strength of $1.5 \cdot 10^8$ V/cm: electron charge density distribution and a collapsing core fragment for Q1D-1 (a, b) model and Q1D-2 (c, d).

this structure is separated only partially, however, separation of a part of graphene caused significant breakdown of the tube core. Thus, the field not only pulls the graphene, but tries to break the tube–graphene contact joint. With the increase in the field strength up to $\sim 2 \cdot 10^8$ V/cm, the graphene is separated completely.

At lower strengths $\sim 1 \cdot 10^8$ V/cm, partial demolition is also observed after the first picosecond of the molecular dynamic simulation. However, partial breakdowns in the graphene–tube contact area continue to exist further and the structure is not broken more. DOS profile changes for both structures in the external field are identical. The Fermi level is shifted towards negative values. Fig. 4 shows the DOS curves for Q1D-1 model for three various strengths. DOS profile shift together with the Fermi level can be seen. A similar pattern can be also observed for Q1D-2 structure.

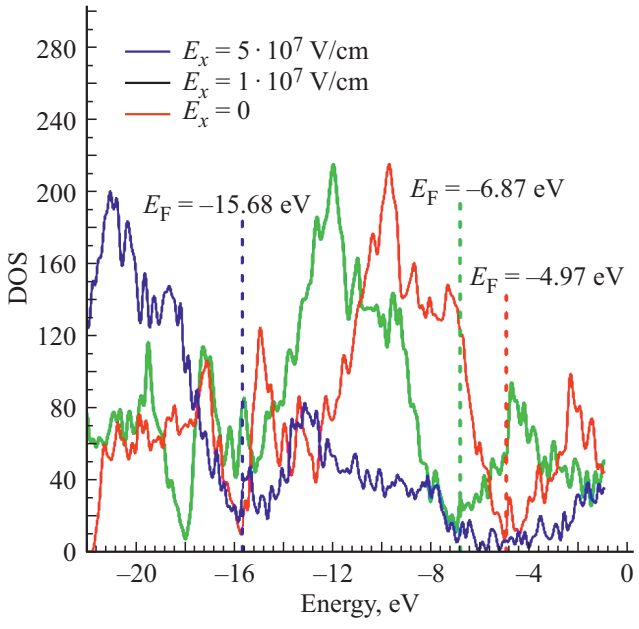

Figure 4. Density of electronic states of Q1D-1v quasi-1D-structure at different external electric field strengths.

6. Conclusion

New knowledge has been obtained regarding the influence of strong electric fields on the atomic and electron structure of graphene/nanotube quasi-1D-structures to be used in field-emission electronic devices. Two topological types of composite models have been discussed: 1) based on chiral nanotube (6,5) and graphene flakes; 2) based on chiral nanotube (6,5) and „armchair"-type graphene nanoribbon. It has been shown that for both models, unsymmetrical distribution of non-hexagonal elements in the graphene–nanotube contact area is typical and is

caused by the chiral tube structure. It has been found that, despite the semiconductor conductivity nature of the tube (6,5) and armchair graphene nanoribbon, the hybrid quasi-1D-structures obtained from them become conductive as a result of partial charge flow from the nanotube to the graphene nanoribbon caused by sp^3-hybridization of atom electron clouds in the graphene−nanotube contact area. Critical electric field strengths that cause demolition of the quasi-1D-structures have been defined for the first time. It has been found that partial structure demolition in the form of graphene fragment separation from the nanotube and local breakdown of bonds between the nanotube atoms in the quasi-1D-structures began at a field strength of $1.5 \cdot 10^8$ V/cm. It has been shown that for both graphene/nanotube quasi-1D-structure models, the Fermi level shift towards the negative energy range is observed in the external field. The new knowledge is important for evaluation of field-emission properties of similar quasi-1D-structures which may be used as a field-emission edge cathode.

Funding

The research was supported by a financial grant provided by the Russian Science Foundation (project No. 21-19-00226).

Conflict of interest

The authors declare that they have no conflict of interest.

References

[1] A.K. Geim, K.S. Novoselov. Nature Mater. **6**, 183 (2007).
[2] V. Georgakilas, J.A. Perman, J. Tucek, R. Zboril. Chem. Rev. **115**, *11*, 4744 (2015).
[3] M.F.L. De Volder, S.H. Tawfick, R.H. Baughman, A.J. Hart. Science **339**, *6119*, 535 (2013).
[4] V.T. Dang, D.C. Nguyen, T.T. Cao, P.H. Le, D.L. Tran, N.M. Phan, V.C. Nguyen. Adv. Nat. Sci.: Nanosci. Nanotechnol. **7**, *3*, 033002 (2016).
[5] Y. Li, Q. Ai, L. Mao, J. Guo, T. Gong, Y. Lin, G. Wu, W. Huang, X. Zhang. Sci. Rep. **11**, 21006 (2021).
[6] R. Ghosh, T. Maruyama, H. Kondo, K. Kimoto, T. Nagai, S. Iijima. Chem. Commun. **51**, *43*, 8974 (2015).
[7] E. Shi, H. Li, L. Yang, J. Hou, Y. Li, L. Li, A. Cao, Y. Fang. Adv. Mater. **27**, *4*, 682 (2015)
[8] L.A. Chernozatonsky, P.B. Sorokin, A.A. Artyukh. Uspekhi khimii **83**, *3*, 251 (2014) (in Russian).
[9] A.L. Gorkina, A.P. Tsapenko, E.P. Gilshteyn, T.S. Koltsova, T.V. Larionova, A. Talyzin, A.S. Anisimov, I.V. Anoshkin, E.I. Kauppinen, O.V. Tolochko, A.G. Nasibulin. Carbon **100**, 501 (2016).
[10] W. Du, Z. Ahmed, Q. Wang, C. Yu, Z. Feng, G. Li, M. Zhang, C. Zhou, R. Senegor, C.Y. Yang. 2D Mater. **6**, *4*, 042005 (2019).
[11] G.K. Dimitrakakis, E. Tylianakis, G.E. Froudakis. Nano Lett. **8**, *10*, 3166 (2008).
[12] W. Wang, M. Ozkan, C.S. Ozkan. J. Mater. Chem. A **4**, *9*, 3356 (2016).
[13] M.Q. Zhao, X.F. Liu, Q. Zhang, G.L. Tian, J.Q. Huang, W. Zhu, F. Wei. ACS Nano **6**, *12*, 10759 (2012).
[14] Y. Zhu, L. Li, C. Zhang, G. Casillas, Z. Sun, Z. Yan, G. Ruan, Z. Peng, A.R.O. Raji, C. Kittrell, R.H. Hauge, J.M. Tour. Nature Commun. **3**, 1225 (2012).
[15] F. Du, D. Yu, L. Dai, S. Ganguli, V. Varshney, A.K. Roy. Chem. Mater. **23**, *21*, 4810 (2011).
[16] A. Hassani, M.T.H. Mosavian, A. Ahmadpour, N. Farhadian. J. Chem. Phys. **142**, *23*, 234704 (2015).
[17] I.N. Kholmanov, C.W. Magnuson, R. Piner, J.Y. Kim, A.E. Aliev, C. Tan, T.Y. Kim, A.A. Zakhidov, G. Sberveglieri, R.H. Baughman, R.S. Ruoff. Adv. Mater. **27**, *19*, 3053 (2015).
[18] F. Tristán-López, A. Morelos-Gómez, S.M. Vega-Díaz, M.L. García-Betancourt, N. Perea-López, A.L. Elías, H. Muramatsu, R. Cruz-Silva, S. Tsuruoka, Y.A. Kim, T. Hayahsi, K. Kaneko, M. Endo, M. Terrones. ACS Nano **7**, *12*, 10788 (2013).
[19] S.H. Kim, W. Song, M.W. Jung, M.A. Kang, K. Kim, S.J. Chang, S.S. Lee, J. Lim, J. Hwang, S. Myung, K.S. An. Adv. Mater. **26**, *25*, 4247 (2014).
[20] X. Gan, R. Lv, J. Bai, Z. Zhang, J. Wei, Z.H. Huang, H. Zhu, F. Kang, M. Terrones. 2D Mater. **2**, *3*, 034003 (2015).
[21] Z. Yan, Z. Peng, G. Casillas, J. Lin, C. Xiang, H. Zhou, Y. Yang, G. Ruan, A.R. Raji, E.L. Samuel, R.H. Hauge, M.J. Yacaman, J.M. Tour. ACS Nano **8**, *5*, 5061 (2014).
[22] Z. Chen, T. Lv, Y. Yao, H. Li, N. Li, Y. Yang, K. Liu, G. Qian, X. Wang, T. Chen. J. Mater. Chem. A **7**, *43*, 24792 (2019).
[23] X. Yang, D. Yu, B. Cao, A.C. To. ACS Appl. Mater. Interfaces **9**, *1*, 29 (2017).
[24] K. Duan, L. Li, Y. Hu, X. Wang. Sci. Rep. **7**, 14012 (2017).
[25] A. Pedrielli, S. Taioli, G. Garberoglio, N.M. Pugno. Micropor. Mesopor. Mater. **257**, 222 (2018).
[26] J. Chen, J.H. Walther, P. Koumoutsakos. Nanotechnology **27**, 465705 (2016).
[27] Y. Liu, Y. Liu, S. Qin, Y. Xu, R. Zhang, F. Wang. Nano Res. **10**, *6*, 1880 (2016).
[28] B. Cai, H. Yin, T. Huo, J. Ma, Z. Di, M. Li, N. Hu, Z. Yang, Y. Zhang, Y. Su. J. Mater. Chem. C **8**, *10*, 3386 (2020).
[29] B. Liu, M. Alamri, M. Walsh, J.L. Doolin, C.L. Berrie, J.Z. Wu. ACS Appl. Mater. Interfaces **12**, *47*, 53115 (2020).
[30] H. Kim, J. Kim, H.S. Jeong, H. Kim, H. Lee, J.M. Ha, S.M. Choi, T.H. Kim, Y.C. Nah, T.J. Shin, J. Bang, S.K. Satijag, J. Koo. Chem. Commun. **54**, *41*, 5229 (2018).
[31] Q. Cheng, J. Tang, J. Ma, H. Zhang, N. Shinyaa, L.-C. Qinc. Phys. Chem. Chem. Phys. **13**, *39*, 17615 (2011).
[32] R.T. Lv, E. Cruz-Silva, M. Terrones. ACS Nano 2014, **8**, *5*, 4061.
[33] X.L. Li, J.W. Sha, S.K. Lee, Y.L. Li, Y.S. Ji, Y.J. Zhao, J.M. Tour. ACS Nano **10**, *8*, 7307 (2016).
[34] L. Cai, X. Xue, M. Liu, H. Li, X. Zhou, G. Yu. APL Materials **9**, *4*, 041110 (2021).
[35] E.F. Sheka, L.A. Chernozatonsky, A.A. Artyukh. Pis'ma v ZhETF **89**, *7*, 412 (2009) (in Russian).
[36] L.A. Chernozatonskii, P.B. Sorokin. ECS Trans. **19**, *13*, 35 (2009).
[37] E.F. Sheka, L.A. Chernozatonskii. J. Comput. Theor. Nanosci. **7**, *9*, 1814 (2010).
[38] A.A. Artyukh, L.A. Chernozatonskii, P.B. Sorokin. Phys. Status Solidi B **247**, *11−12*, 2927 (2010).

[39] V.V. Ivanovskaya, A. Zobelli, P. Wagner, M.I. Heggie, P.R. Briddon, M.J. Rayson, C.P. Ewels. Phys. Rev. Lett. **107**, *6*, 065502 (2011).
[40] M.A. Akhukov, S. Yuan, A. Fasolino, M.I. Katsnelson. New J. Phys. **14**, 123012 (2012).
[41] O.E. Glukhova, I.S. Nefedov, A.S. Shalin, M.M. Slepchenkov. Beilstein J. Nanotechnol. **9**, 1321 (2018).
[42] J. Gonga, P. Yang. RSC Adv. **4**, *38*, 19622 (2014).
[43] T. Matsumoto, S. Saito. J. Phys. Soc. Jpn. **71**, 2765 (2002).
[44] Y. Mao, J. Zhong. New J. Phys. **11**, 093002 (2009).
[45] F.D. Novaes, R. Rurali, P. Ordejón. ACS Nano **4**, *12*, 7596 (2010).
[46] J. Chen, J.H. Walther, P. Koumoutsakos Adv. Funct. Mater. **25**, 7539 (2015).
[47] V. Varshney, S.S. Patnaik, A.K. Roy, G. Froudakis, B.L. Farmer. ACS Nano **4**, *2*, 1153 (2010).
[48] Z. Zhang, A. Kutana, A. Roy, B.I. Yakobson. J. Phys. Chem. C **121**, *2*, 1257 (2017).
[49] D.D. Nguyen, R.N. Tiwari, Y. Matsuoka, G. Hashimoto, E. Rokuta, Y. Chen, Y.L. Chueh, M. Yoshimura. ACS Appl. Mater. Interfaces **6**, *12*, 9071 (2014).
[50] M. Song, P. Xu, Y. Song, X. Wang, Z. Li, X. Shang, H. Wu, P. Zhao, M. Wang. AIP Adv. **5**, *9*, 097130 (2015).
[51] S. Riyajuddin, S. Kumar, K. Soni, S.P. Gaur, D. Badhwar, K. Ghosh. Nanotechnology **30**, *38*, 385702 (2019).
[52] A.T.T. Koh, T. Chen, L. Pan, Z. Sun, D.H.C. Chua. J. Appl. Phys. **113**, *17*, 174909 (2013).
[53] L. Chen, H. He, H. Yu, Y. Cao, D. Lei, Q. Menggen, C. Wu, L. Hu. J. Alloys Compd. **610**, 659 (2014).
[54] X. Hong, W. Shi, H. Zheng, D. Liang. Vacuum **169**, 108917 (2019).
[55] A.Y. Gerasimenko, A.V. Kuksin, Y.P. Shaman, E.P. Kitsyuk, Y.O. Fedorova, A.V. Sysa, A.A. Pavlov, O.E. Glukhova. Nanomaterials **11**, *8*, 1875 (2021).
[56] B. Hourahine, B. Aradi, V. Blum, F. Bonafé, A. Buccheri, C. Camacho, C. Cevallos, M.Y. Deshaye, T. Dumitrică, A. Dominguez, S. Ehlert, M. Elstner, T. van der Heide, J. Hermann, S. Irle, J.J. Kranz, C. Köhler, T. Kowalczyk, T. Kubař, I.S. Lee, V. Lutsker, R.J. Maurer, S.K. Min, I. Mitchell, C. Negre, T.A. Niehaus, A.M.N. Niklasson, A.J. Page, A. Pecchia, G. Penazzi, M.P. Persson, J. Řezáč, C.G. Sánchez, M. Sternberg, M. Stöhr, F. Stuckenberg, A. Tkatchenko, V.W.Z. Yu, T. Frauenheim. J. Chem. Phys. **152**, *12*, 124101 (2020).
[57] H.J. Monkhorst, J.D. Pack. Phys. Rev. B **13**, *12*, 5188 (1976).
[58] A.K. Rappe, C.J. Casewit, K.S. Colwell, W.A. Goddard III, W.M. Skiff. J. Am. Chem. Soc. **114**, *25*, 10024 (1992).
[59] S. Datta. Quantum Transport: Atom to Transistor. Cambridge University Press, N.Y. (2005). 432 p.
[60] B. Aradi, A.M.N. Niklasson, T. Frauenheim. J. Chem. Theory Comput. **11**, *7*, 3357 (2015).
[61] R. Car, M. Parrinello. Phys. Rev. Lett. **55**, *22*, 2471 (1985).